Eur. Phys. J. B **45**, 223–230 (2005)
DOI: 10.1140/epjb/e2005-00177-4

THE EUROPEAN PHYSICAL JOURNAL B

Size and shape dependence of the exchange-bias field in exchange-coupled ferrimagnetic bilayers

M. Ziese[1,a], R. Höhne[1], A. Bollero[1,b], H.-C. Semmelhack[1], P. Esquinazi[1], and K. Zimmer[2]

[1] Division of Superconductivity and Magnetism, University of Leipzig, Linnéstrasse 5, 04103 Leipzig, Germany
[2] Institute for Surface Modification, 04318 Leipzig, Germany

Received 15 September 2004 / Received in final form 20 April 2005
Published online 28 June 2005 –

Abstract. Exchange biasing was studied in an exchange-spring system consisting of two ferrimagnetic films with different coercivity. Magnetite and Co-Fe ferrite were chosen as the soft and hard magnetic bilayer components, respectively. The samples were epitaxially grown on MgO single crystal substrates by pulsed laser deposition. The exchange-bias field was investigated as a function of system size and shape, magnetic field direction and magnetization reversal in the hard layer. A clear dependence of the exchange-bias field on the sample size and shape was found. This was attributed to an interplay between exchange and dipolar energies. Micromagnetic simulations agree with the experimental results.

PACS. 71.70.Gm Exchange interactions – 75.50.Gg Ferrimagnetics – 75.70.-i Magnetic properties of thin films, surfaces, and interfaces

1 Introduction

Exchange biasing refers to the uni-directional magnetic anisotropy observed in a ferromagnet (F)–antiferromagnet (AF) system. This usually results in the shift of the ferromagnetic hysteresis loop along the magnetic field axis by the exchange-bias field H_{EB}. The anisotropy arises from the exchange interaction between AF and F interface spins, for an overview see [1,2]. A similar uni-directional anisotropy is also observed in systems consisting of hard and soft ferro- or ferrimagnets, so-called exchange spring systems [3–6]. In both systems, F–F and F–AF, the exchange interaction is mediated by the interface spins; actually, the all-ferromagnetic system has the same interface structure as the ideal interface between a ferromagnet and an A-type antiferromagnet. In real F–AF systems, however, interface roughness and the use of G-type antiferromagnets lead to a more complex interfacial spin structure than in the case of F–F systems. The complexities are mainly related to the fact that in real F–AF systems the antiferromagnetic spin-structure is close to being compensated such that the global exchange-bias field is much smaller than the ideal value derived by Meiklejohn [7]. Various models have been developed invoking interface roughness [8], polycrystallinity [9] and bulk antiferromagnet domain formation [10] to explain the formation of uncompensated spins at the interface and a finite exchange-bias field. In these F–AF systems the exchange-bias field has been shown to depend on the structure size and layer thickness [11] and the shape anisotropy [12].

In case of exchange-spring systems the situation is simpler in the sense that independent of interface roughness there are always uncompensated spins at the interface that might give rise to exchange coupling. However, since the total energy of a magnetic bilayer system does not only involve exchange and Zeeman terms, but moreover magnetocrystalline anisotropy and dipole-interaction terms, it can be anticipated that the magnitude of the exchange-biasing might depend on external factors such as sample shape and magnetic domain structure. The focus of the present work is the study of the exchange-bias field as a function of sample dimensions, sample shape and – indirectly – domain-structure. A ferrimagnetic exchange-spring system was chosen in order to minimize complications arising from the interfacial spin structure. Actually, few experimental data on F–F coupling in thin films are available. Here $Co_{0.16}Fe_{2.84}O_4/Fe_3O_4$ bilayers were studied. Besides the considerations on the interfacial spin structure this system was chosen for two further reasons: (1) in contrast to F–AF systems the use of F–F systems enables the direct manipulation of the hard magnetic layer by the magnetic field, thus adding an additional experimental parameter and (2) bilayers of this type can be epitaxially grown allowing for a good structural quality throughout the system.

In recent years some studies have focused on Fe_3O_4–$CoFe_2O_4$ bilayer systems [13–15]. Magnetite and $CoFe_2O_4$

[a] e-mail: ziese@physik.uni-leipzig.de
[b] *Present address*: SPINTEC, C.E.A/C.N.R.S, 38054 Grenoble Cedex 9, France

are ferrimagnets with a saturation magnetization of 4 μ_B/f.u. and 3.7 μ_B/f.u., respectively, both crystallizing in the spinel structure. Whereas $CoFe_2O_4$ is an insulator, calculations indicate that the metallic state of magnetite might have a half-metallic structure [16,17]. There are experimental results supporting this [18], but the half-metallicity is still under discussion and arguments using angular momentum coupling rules predict a spin-polarization of only $-2/3$ [19,20]. The relatively large saturation magnetization of Co-ferrite films and its high crystalline anisotropy – at room temperature $K_1 = 3 \times 10^5$ J/m^3 in comparison to $K_1 = -1.1 \times 10^4$ J/m^3 for Fe_3O_4 – lead to square magnetization loops when measuring along the easy axis, thus making them suitable for biasing [13]. These experiments, however, were carried out on large area samples with typical dimensions of 5×5 mm^2. Aim of this work is to study the evolution of the exchange-bias field with the sample dimensions, sample shape and – indirectly – with the change of the magnetic domain structure. For this magnetization measurements on full area films and samples patterned in the form of stripes or dots were performed. The experimental results are further compared to micromagnetic simulations on bilayer systems with different size.

2 Experimental details

Thin film bilayers of nominal composition $Co_{0.16}Fe_{2.84}O_4$–Fe_3O_4 were prepared by pulsed laser deposition from stoichiometric targets onto MgO (001) substrates. Substrate temperature was 430 °C and oxygen background pressure 1.5×10^{-6} mbar. A Lambda-Physik Excimer laser at a wavelength of 248 nm (KrF) operated at a repetition rate of 10 Hz and a pulse energy of 0.6 J was used. The fluence was about 2.5 J/cm^2. The unpatterned films had an area of 5×5 mm^2. Film thickness was determined from profilometer measurements with a total thickness between 200 ± 20 nm and 300 ± 30 nm. Co-Fe ferrite and magnetite films had about the same thickness. The films were investigated using high resolution X-ray diffractometry; this indicated epitaxial growth. Details on the structural characterization are published in [15,21–23]. The samples were subsequently patterned using conventional photolithographic techniques and ion-beam etching. The patterning proceeded in two steps with the fabrication of stripes in the first and of dots in the second step. Stripe widths were 10 μm and 3 μm with spacing between the stripes of 10 μm and 3 μm, respectively. The samples presented in this study are listed in Table 1. The overall magnetic behaviour, especially the shape of the magnetization curves, was the same for all samples.

Magnetization measurements were carried out with a Superconducting Quantum Interference Device (SQUID) magnetometer (Quantum Design MPMS-7). Most measurements were performed at 5 K after field cooling the samples in a field of 4 T applied parallel to one sample edge through the Verwey transition. The magnetic fields applied during the hysteresis loop measurements were always parallel to the field-cooling field.

Table 1. Sample parameters.

Sample	type	bilayer thickness
1	full film	220 nm
2a	full film	280 nm
2b	10 μm stripes	fabricated from 2a
2c	10×10 μm^2 dots	fabricated from 2b
3a	full film	200 nm
3b	3 μm stripes	fabricated from 3a
3c	3×3 μm^2 dots	fabricated from 3b

Atomic force microscopy (AFM) and magnetic force microscopy (MFM) measurements were performed using a Nanoscope IIIa with a Dimension 3000 scanning probe microscope (Digital Instruments) with an extender electronics module. Standard MESP (magnetically coated etched silicon probe) tips were used. The topographic and magnetic information was collected using lift mode, i.e. during a first scan in contact (AFM) the topography was recorded and in a second scan the tip was moved across the sample with a constant height over the surface to detect the magnetic response, see e.g. [24]. A lift height of 50 nm was chosen.

Micromagnetic simulations were performed with the three-dimensional micromagnetic solver OXSII developed within the Object Oriented Micromagnetic Framework (OOMMF) [25]. Parameters used were a saturation magnetization $M_s = 5 \times 10^5$ A/m for both layers, an exchange stiffness A of 12×10^{-12} J/m for both layers and across the interface, an uniaxial magnetocrystalline anisotropy with $K_u = 6 \times 10^4$ J/m^3 for the soft layer (top layer) [26] and $K_u = 30 \times 10^4$ J/m^3 for the hard layer (bottom layer). The saturation magnetization chosen is close to that of magnetite. It is believed that variations in the saturation magnetization do not change the micromagnetic patterns significantly. The exchange stiffness was estimated from magnetocrystalline anisotropy constant and domain-wall width [27] and is thought to be rather unaffected by the Co-doping. The low temperature uniaxial anisotropy constant was determined for magnetite films by torque magnetometry [26]; in case of the hard magnetic layer a value was chosen such that a reasonable switching field was obtained.

Simulations were carried out for pillars of height 100 nm and areas ranging between 3×3 μm^2 and 30×30 nm^2. A regular mesh with $30 \times 30 \times 10$ cells was used in all cases, whereas additional calculations with a regular mesh of $100 \times 100 \times 10$ were carried out for the 3×3 μm^2, 1×1 μm^2 and 300×300 nm^2 samples. The hysteresis loops did not depend on cell size in case of the 300×300 nm^2 sample and were quite similar for the 1×1 μm^2 sample, whereas significant deviations were seen for the 3×3 μm^2 sample. We are confident that the results of the calculations using $100 \times 100 \times 10$ cells are accurate up to system sizes of 1×1 μm^2, whereas the accuracy of the 3×3 μm^2 result could not be evaluated, since we cannot perform simulations with larger system sizes. The magnetic field was

applied within the film plane under an angle of about 3° with respect to the uniaxial axis.

The interlayer exchange observed in the micromagnetic simulations stems from the exchange interaction between single magnetic cells. In the continuum approximation the exchange energy per sample volume V is given by

$$E_{ex}/V = A(\nabla \hat{m})^2 \tag{1}$$

with the exchange stiffness A and the unit magnetization vector field $\hat{m}$. In the simulations this is discretized and the exchange-energy density contribution from cell i is given by [25]

$$E_{ex,i} = \sum_{j \in N_i} A_{ij} \frac{\hat{m}_i \cdot (\hat{m}_i - \hat{m}_j)}{\Delta_{ij}^2} \tag{2}$$

where N_i is the set consisting of the six cells nearest to cell i, A_{ij} is the exchange coefficient between cells i and j and Δ_{ij} is the discretization step size between cell i and cell j.

The results will show that the exchange-bias field is influenced by the dipolar energy

$$E_d = -\frac{1}{2} \int_V \mu_0 \boldsymbol{M} \cdot \boldsymbol{H}_d dV, \tag{3}$$

where $\boldsymbol{H}_d$ denotes the stray field generated by the sample magnetization; see [25] for details on the discretization.

3 Results

3.1 General phenomenology

An AFM/MFM image of sample 3b in zero field is shown in Figure 1. On the left side the topography is shown in a three dimensional view, in top view and in a cross-sectional cut. The stripe structure is clearly discernible with a height of the stripes of 800 nm. This demonstrates that the ion-beam etching was carried out deep into the substrate and the magnetic material is clearly separated. The corresponding MFM images are shown on the right side. In comparison to the topography additional structures can be seen which are attributed to magnetic domain signals. Since the bilayers have in-plane magnetic anisotropy, the MFM signals appear especially at the sides of the stripes, where the stray fields are largest.

In the following magnetization hysteresis loops will be presented. In order to determine the exchange-bias field H_{EB} full and minor hysteresis loops were recorded. Here a full loop refers to a measurement traversing a field range with return fields of equal magnitude, but opposite polarity chosen such that both layers are in technical saturation. A minor loop is usually an asymmetric hysteresis loop with return fields chosen such that the hard magnetic layer is not reversed. The inset to Figure 2 shows a schematic minor loop. In the following the switching (or reversal fields) of the minor loop will be denoted by H_{S+} and H_{S-} and the return fields of the loop by H_{R+}

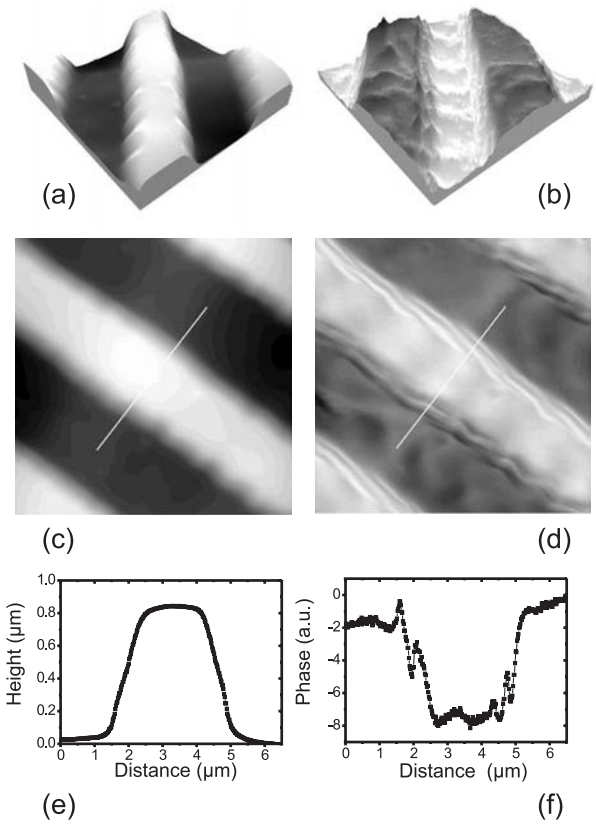

Fig. 1. Left: AFM image of sample 3b in (a) a three dimensional view, (c) a top view and (e) a cross-sectional cut. Scan area is 10×10 μm^2 and z-scale 1.1 μm. Right: Corresponding MFM images. Phase scale is 13°. Note that the MFM images (b) and (d) are shown with inverted gray scales in order to demonstrate the magnetic features more clearly. The cross-sections were obtained along the white lines shown in (c) and (d).

and H_{R-}. The coercive field of the soft layer H_C was defined as the half width of the minor loop:

$$H_C = (H_{S+} - H_{S-})/2 \tag{4}$$

The magnetic field was always applied within the plane of the layers.

Full hysteresis loops measured at 5 K and 300 K on sample 3a are shown in Figure 2a. Whereas at 300 K the magnetization reversal of the magnetite layer influences the magnetization of the Co-Fe ferrite layer leading to a simultaneous magnetization reversal, at 5 K a completely separate reversal of the two layers and a sharp switching of the magnetite layer was observed. The measurements at 5 K were performed after field cooling the bilayer in an applied field of 4 T through the Verwey transition. This induces an uniaxial magnetocrystalline anisotropy in the magnetite layer along the magnetization direction [26,28]. Unless indicated otherwise all other measurements were performed at 5 K after field cooling.

Figure 2b shows a zoom of a full and a minor hysteresis loop of sample 3a at 5 K. The minor loop is clearly shifted on the field axis towards negative fields, i.e. an

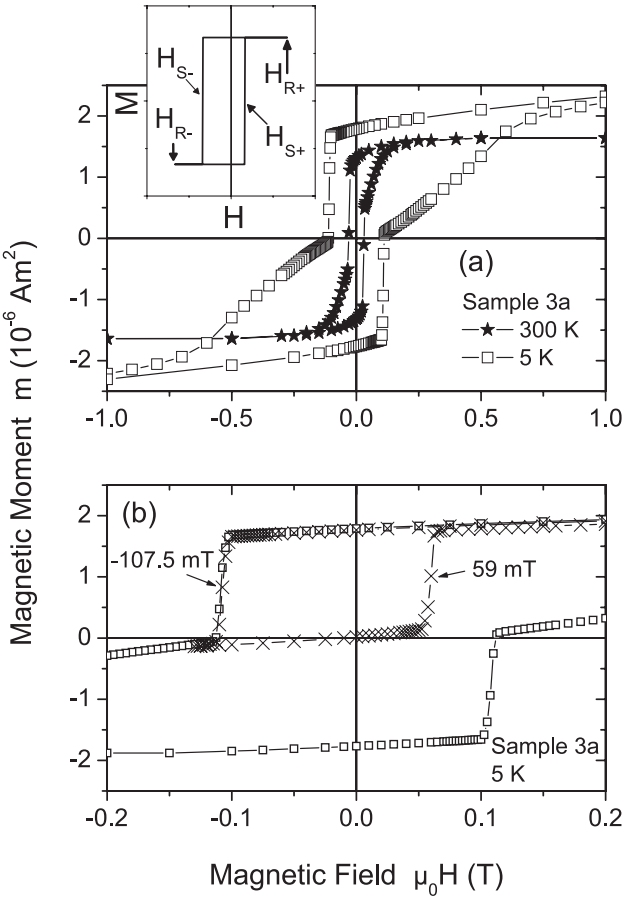

Fig. 2. (a) Full hysteresis loops recorded for sample 3a at 5 K and 300 K. The measurement at 5 K was performed after field cooling the bilayer through the Verwey transition in an applied magnetic field of 4 T. (b) Full and minor hysteresis loops measured on sample 3a at 5 K after field cooling. The switching fields are indicated. The inset shows a schematic minor loop with the definition of the switching fields H_{S+} and H_{S-} and the return fields H_{R+} and H_{R-}.

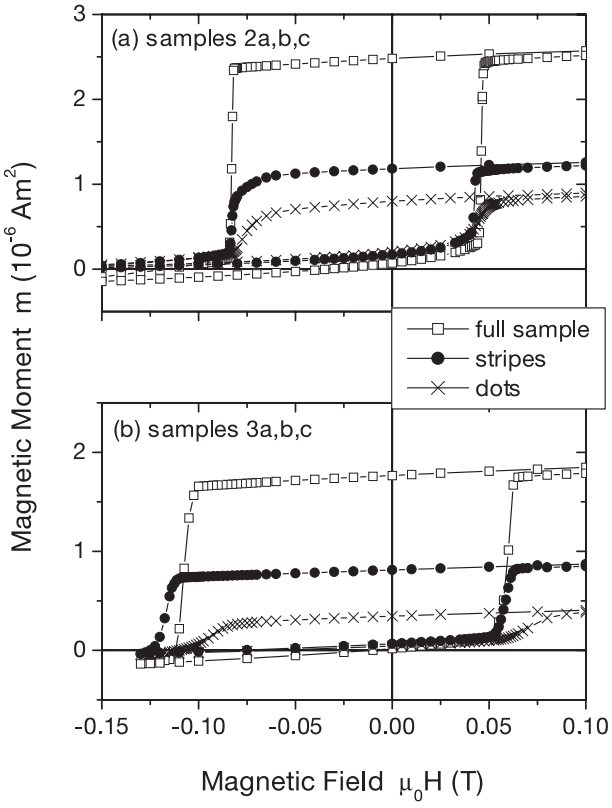

Fig. 3. (a) Minor magnetic moment hysteresis loops for the original sample 2a and the patterned samples 2b and 2c measured at 5 K after field cooling through the Verwey transition. (b) Minor loops of samples 3a, 3b and 3c measured at 5 K after field cooling. In both cases the magnetic field was applied parallel to the stripes.

exchange-bias field H_{EB} is present in this bilayer. The exchange-bias field is defined as

$$H_{EB} = |H_{S+} + H_{S-}|/2 \tag{5}$$

with $\mu_0 H_{EB} \simeq 24$ mT in this case.

3.2 Size effects

One central result of the present study is shown in Figure 3. There minor hysteresis loops measured at 5 K for samples 2a-c and 3a-c are shown. It can be seen that in going from the full film to stripes and finally dots the magnetic moment decreases by approximately a factor of two in each step. This is in agreement with the amount of sample material removed and indicates that the patterning process does not introduce excessive damage to the bilayers. The hysteresis loops of the patterned samples show some shearing that is attributed to the switching field distribution of the stripes and dots. The minor hysteresis loops demonstrate that the switching fields H_{S+} and H_{S-} change with the areal size of the ferrimagnetic entities. This is especially pronounced for sample 3. From the switching fields and using equation (5) values for the exchange-bias fields of $\mu_0 H_{EB} = 19$, 20 and 16 mT for samples 2a, 2b and 2c and $\mu_0 H_{EB} = 24$, 29 and 11 mT for samples 3a, 3b and 3c were obtained, respectively. In both cases stripe samples show higher and dots clearly lower values of H_{EB}. This is a strong indication that the changes in the exchange-bias field are not caused by damage introduced by the patterning process, but are due to changes in the size and shape of the magnetic elements and to changes in the magnetic domain structure. The coercive fields of the magnetite layer depend only weakly on the structure size with $\mu_0 H_C = 64$, 63 and 59 mT for samples 2a, 2b and 2c and $\mu_0 H_C = 84$, 88 and 83 mT for samples 3a, 3b and 3c, respectively.

In order to study the influence of the magnetic domain structure on the exchange-bias field the stripe samples were measured in magnetic fields applied parallel and perpendicular to the stripes. In Figure 4 the minor magnetic moment hysteresis loops measured at 5 K for sample 2b are presented. The results show a clear dependence of the minor loops on the direction of the applied field. The

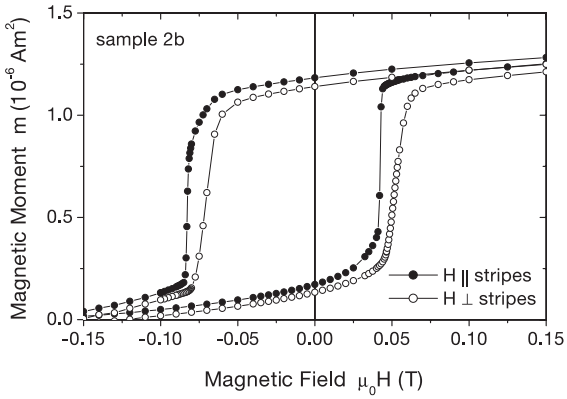

Fig. 4. Comparison of the minor loops of sample 2b measured at 5 K after field cooling in magnetic fields applied parallel and perpendicular to the stripes.

exchange-bias field depends strongly on the field direction with $\mu_0 H_{EB} = 20$ mT for fields parallel and 9 mT for fields perpendicular to the stripes. This behaviour demonstrates the influence of the different magnetic domain structures on H_{EB}. At the same time the coercive field of the magnetite layer is unchanged with 62 mT in longitudinal and 61 mT in transverse orientation.

The change in the exchange-bias field is attributed to an interplay between dipolar and interfacial exchange energy. In case of the stripes in parallel and perpendicular field this is especially clear. The dipolar energy of the perpendicular configuration is higher than in the parallel configuration, since the demagnetizing factor is larger for this field direction. This raises the total energy of the system and leads to a smaller exchange-bias field in the perpendicular orientation in order to minimize the stray-field energy. The same argument explains the decrease of the exchange-bias field when going from stripes in parallel field to dots.

3.3 The influence of re-magnetization processes

Since exchange biasing must be related to exchange interactions across the interface, the hard magnetic layer experiences an exchange field exerted by the soft layer in addition to the external magnetic field. It is therefore expected that magnetization reversal processes in the hard layer will be initiated at the interface. In order to prove this the hard layer was partially re-magnetized and the exchange-bias field was measured as a function of the reversed magnetic moment in the hard layer. The partial reversal of the hard magnetic layer was achieved by two methods, namely the application of return fields H_{R-} with different magnitude (direct magnetization reversal by the applied field) as well as waiting time measurements (for similar measurements on F–AF systems see [29,30]). In the waiting time experiments the measurement of the minor hysteresis loop is interrupted on reaching the desired return field H_{R-} (-87.5 mT in this case) and is resumed after a defined waiting time t_w. Results of both experiments are shown

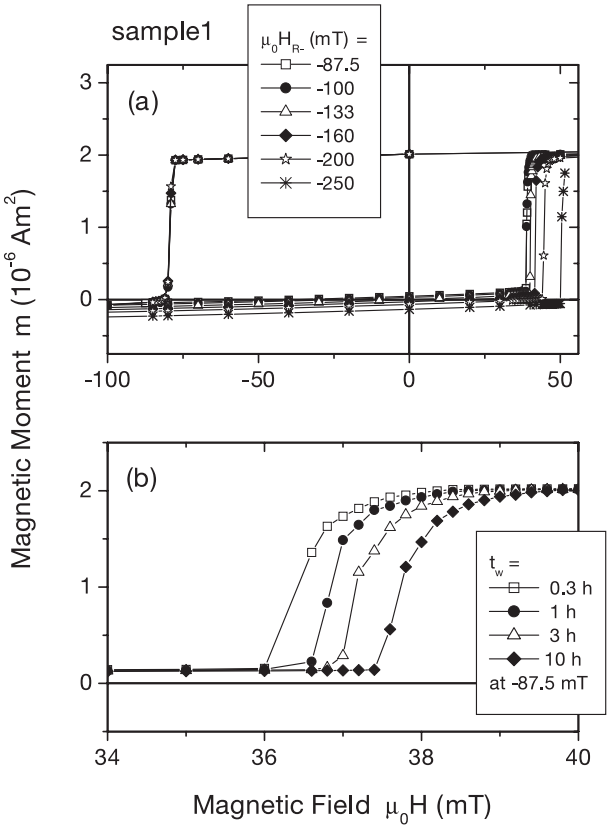

Fig. 5. (a) Minor hysteresis loops measured for sample 1 at 5 K and at various return fields H_{R-}. (b) Minor loops measured for sample 1 at 5 K. At the return field $\mu_0 H_{R-} = -87.5$ mT the measurement was interrupted for a waiting time t_w indicated in the figure.

in Figure 5. In both cases the switching field H_{S-} is unaffected, whereas H_{S+} increases with decreasing return field H_{R-} and increasing waiting time. As expected H_{EB} decreases with increasing partial magnetization reversal of the hard layer. The normalized exchange-bias field is plotted as a function of the fractional change in the hard layer magnetization

$$\Delta M = M(-87.5\,\mathrm{mT}, t_w = 0) - M(H, t_w) \qquad (6)$$

in Figure 6. The relaxation measurements lead to very small magnetization changes such that only the data point for a waiting time of 10 h is shown. That value is in good agreement with the extrapolated trend from the field reversal measurements. The exchange-bias field decreases strongly in a non-linear manner with the fractional magnetization change in the hard layer. This gives a strong indication that magnetization reversal in the hard layer starts at the interface, since in this case the exchange field exerted by the hard layer should decrease stronger than the hard layer magnetization.

3.4 Micromagnetic modelling

The micromagnetic simulations have been used to model the magnetization hysteresis loop and the magnetic

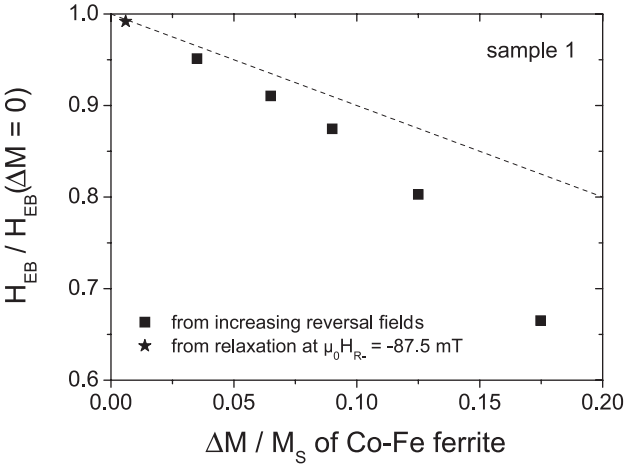

Fig. 6. Relative decrease of the exchange-bias field H_{EB} as a function of the relative reversal of the hard layer magnetization. The reversal was effected by using different return fields H_{R-} or magnetization relaxation due to waiting for t_w at $\mu_0 H_{R-} = -87.5$ mT. If reversal would occur randomly throughout the volume of the hard layer a dependence $\Delta H_{EB}/H_{EB} = 1 - \Delta M/M_S$ as indicated by the dashed line would be expected.

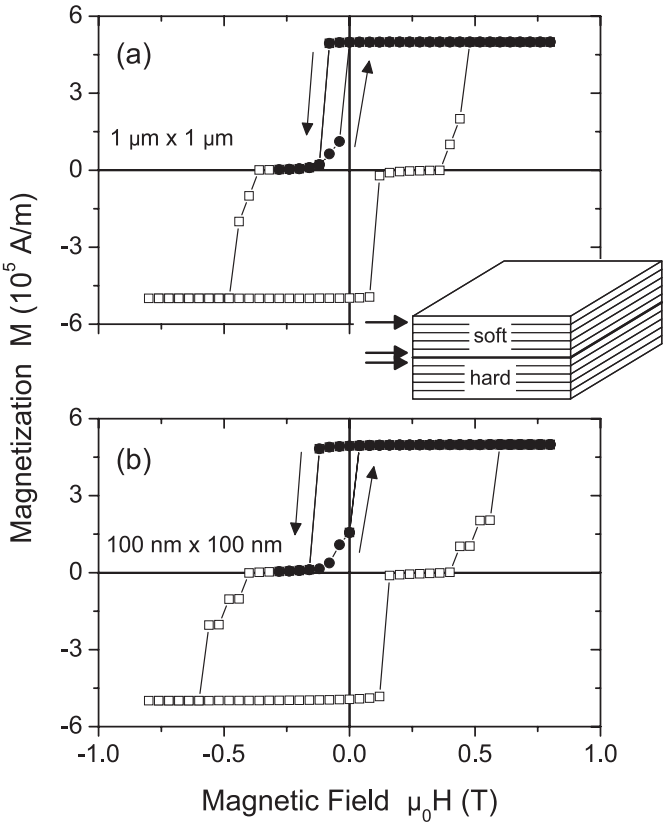

Fig. 7. Magnetization hysteresis loops obtained from micromagnetic simulations of a 100 nm thick bilayer for an areal size of (a) 1×1 μm^2 (mesh $100 \times 100 \times 10$) and (b) 0.1×0.1 μm^2 (mesh $30 \times 30 \times 10$). In both cases a full and a minor hysteresis loop are shown. The inset shows a sketch of the micromagnetic structure indicating the soft and the hard magnetic layers and the vertical mesh that divides the system into ten layers. The arrows indicate the layers whose magnetization distribution is shown in Figure 9.

moment distribution of the bilayer samples. The system sizes chosen are mostly smaller than the system sizes realized experimentally. This is due to limitations in computing time that forbid the treatment of large macroscopic samples. However, the simulations show trends consistent with the experimental data and are therefore a vital extrapolation of the experimentally accessible size regime.

Figure 7 shows both computed full and minor hysteresis loops for (a) 1×1 μm^2 and (b) 0.1×0.1 μm^2 large bilayers. In both cases a separate switching of the layers is seen and overall the simulated data are quite similar to the measured magnetization curves. Exchange biasing is clearly present. However, both the coercive field and the exchange-bias field are somewhat overestimated. This might be due to the ideally flat interface that was assumed in the simulations. Since the primary focus is on the evolution of the magnetic structure and exchange-bias field with sample size, this overestimation should not be of major concern.

Figure 8 shows the exchange-bias field H_{EB}, the coercive field of the magnetite layer H_C and the switching field H_{S+} as a function of bilayer size as determined from the micromagnetic simulations. Data for regular meshes of $30 \times 30 \times 10$ and $100 \times 100 \times 10$ are presented to demonstrate the influence of the micromagnetic cell size. H_{EB} decreases with decreasing sample size down to 300 nm and increases again. The decrease of H_{EB} for sizes in the range between 3 μm and 300 nm is consistent with the experimental observation when going from full films to 3 μm or 10 μm dots. The coercive field H_c shows some increase below a bilayer size of 1 μm, possibly due to configurational anisotropy, before decreasing for the smallest sample.

The magnetization reversal mechanisms can be studied in more detail by an analysis of the magnetization distribution. All micromagnetic simulations were performed with a micromagnetic cell height of 10 nm, such that ten different cross-sections through the bilayers can be defined. Three of these were selected, namely the top and bottom cross-sections of the soft layer and the top one of the hard layer (see inset to Fig. 7), and are displayed at two different magnetic fields in Figure 9 for the 100 nm bilayer. In the initial state the magnetization in both layers was saturated in the positive field direction. The magnetic reverse fields are chosen close to the switching field H_{S-} such that the soft layer is almost fully reversed for the smaller field and is in the reversal process for the larger field. In case of bilayers with size of 300 nm and below, the reversal process is clearly coherent, for larger samples the micromagnetic simulations indicate an incoherent reversal process. The transition from an incoherent to a coherent magnetization reversal mechanism might occur in the size range between 300 nm and 1 μm.

Main result from the micromagnetic simulations is the clear observation of a size dependence of the exchange-bias field. Since the interface magnetic parameters

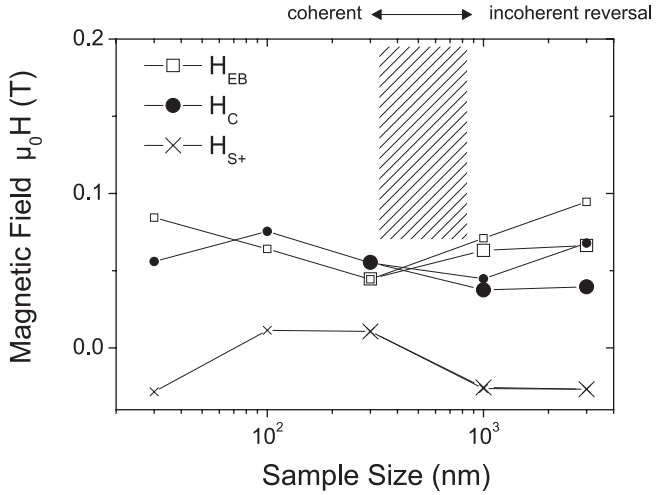

Fig. 8. Exchange-bias field H_{EB}, coercive field H_C and switching field H_{S+} as a function of bilayer size. These data were determined from the micromagnetic simulations. Small and large symbols refer to calculations using a regular mesh of $30\times30\times10$ and $100 \times 100 \times 10$, respectively. The hatched area indicates the size range, where the transition from coherent to incoherent reversal occurs.

between hard and soft layer were chosen identical for all five simulated samples, this size dependence must arise from the different sample shape and magnetic domain states. It is driven by the dependence of the dipolar energy on the system shape. This is in agreement with the experimental data.

4 Discussion and conclusions

A clear exchange-biasing field H_{EB} was measured both in samples with full film area as well as in patterned films. In samples with an increased demagnetizing factor – i.e. in films with reduced size consisting of dots and in stripes in perpendicular field – H_{EB} is clearly reduced. The decrease of the exchange-bias field is attributed to the interplay of dipolar and exchange energy. When the dipolar energy is increased by a change of the sample shape, it is energetically more favourable for the bilayer system to reverse the soft magnetic layer at smaller absolute values of the reverse bias field, thus decreasing the exchange-bias field.

H_{EB} decreases strongly with small magnetization changes of the harder Co-Fe ferrite layer; this change was brought about by relaxation at constant applied field or by a gradual increase of the absolute value of the return field. Obviously the magnetization reversal of the hard layer begins in sample parts near the interface. This is also supported by the micromagnetic simulations.

In summary, we conclude that H_{EB} depends not only on the properties of the interface, but additionally on the magnetic structure of both layers which is strongly influenced by sample size and shape.

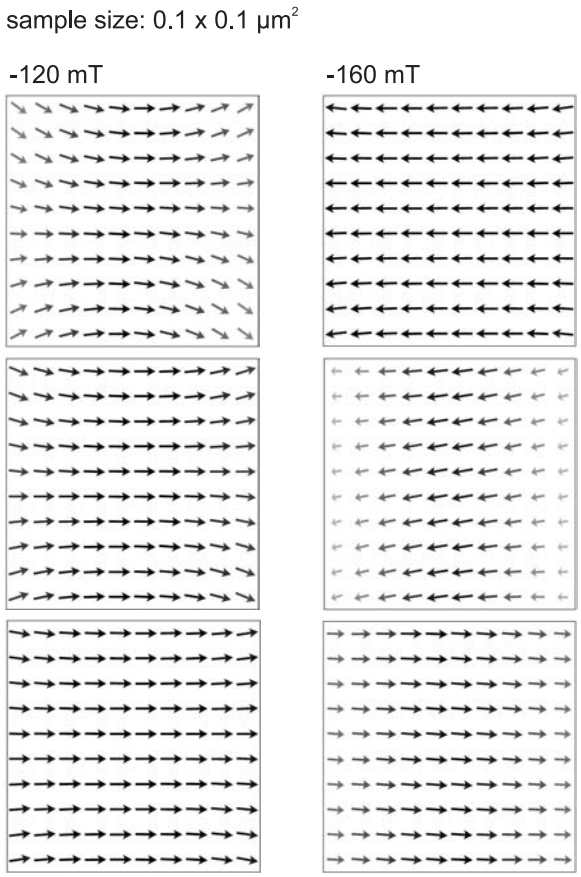

Fig. 9. Magnetic moment distributions determined in three cross sections of the 0.1×0.1 μm^2 bilayer at two reverse bias fields close to the switching field H_{S-}. The upper row shows the magnetic dipole distribution in the top section of the soft layer, the middle row in the bottom section of the soft layer and the lower row in the top section of the hard layer, respectively.

This work was supported by the DFG under Contract No. DFG ES 86/7-3 within the Forschergruppe "Oxidische Grenzflächen".

References

1. J. Nogués, I.K. Schuller, J. Magn. Magn. Mater. **192**, 203 (1999)
2. M. Kiwi. J. Magn. Magn. Mater. **234**, 584 (2001)
3. E.E. Fullerton, J.S. Jiang, M. Grimsditch, C.H. Sowers, S.D. Bader, Phys. Rev. B **58**, 12193 (1998)
4. W. Hahn, M. Loewenhaupt, Y.Y. Huang, G.P. Felcher, S.S.P. Parkin, Phys. Rev. B **52**, 16041 (1995)
5. S. Mangin, F. Montaigne, A. Schuhl, Phys. Rev. B **68**, 140404 (2003)
6. F. Canet, C. Bellouard, L. Joly, S. Mangin, Phys. Rev. B **69**, 094402 (2004)
7. W.H. Meiklejohn, J. Appl. Phys. **33**, 1328 (1962)
8. A.P. Malozemoff, Phys. Rev. B **35**, 3679 (1987)
9. M.D. Stiles, R.D. McMichael, Phys. Rev. B **59**, 3722 (1999)

10. P. Miltényi, M. Gierlings, J. Keller, B. Beschoten, G. Güntherodt, U. Nowak, K.D. Usadel, Phys. Rev. Lett. **84**, 4224 (2000)
11. V. Baltz, J. Sort, S. Landis, B. Rodmacq, B. Dieny, Phys. Rev. Lett. **94**, 117201 (2005)
12. A. Hoffmann, M. Grimsditch, J.E. Pearson, J. Nogués, W.A.A. Macedo, I.K. Schuller, Phys. Rev. B **67**, 220406 (2003)
13. Y. Suzuki, R.B. van Dover, V. Korenivski, D. Werder, C.H. Chen, R.J. Felder, Mater. Res. Soc. Symp. Proc. **401**, 473 (1996)
14. P.A.A. van der Heijden, P.J.H. Bloemen, J.M. Metselaar, R.M. Wolf, J.M. Gaines, J.T.W.M. van Eemeren, P.J. van der Zaag, W.J.M. de Jonge, Phys. Rev. B **55**, 11569 (1997)
15. C.A. Kleint, M.K. Krause, R. Höhne, T. Walter, H.C. Semmelhack, M. Lorenz, P. Esquinazi, J. Appl. Phys. **84**, 5097 (1998)
16. M. Pénicaud, B. Siberchicot, C.B. Sommers, J. Kübler, J. Magn. Magn. Mater. **103**, 212 (1992)
17. A. Yanase, N. Hamada, J. Phys. Soc. Jpn **68**, 1607 (1999)
18. Yu. S. Dedkov, U. Rüdiger, G. Güntherodt, Phys. Rev. B **65**, 064417 (2002)
19. S.F. Alvarado, P.S. Bagus, Phys. Lett. A **67**, 397 (1978)
20. C. Srinitiwarawong, G. Gehring, J. Phys.: Condens. Matter **13**, 7987 (2001)
21. C.A. Kleint, H.C. Semmelhack, M. Lorenz, M.K. Krause, J. Magn. Magn. Mater. **725**, 140-144 (1995)
22. C.A. Kleint, M.K. Krause, R. Höhne, M. Lorenz, H.C. Semmelhack, A. Schneider, D. Hesse, H. Sieber, J. Taubert, W. Andrä, J. Phys. IV France **7**, C1–593 (1997)
23. A. Bollero, M. Ziese, R. Höhne, H.C. Semmelhack, U. Köhler, A. Setzer, P. Esquinazi, J. Magn. Magn. Mater. **285**, 279 (2005)
24. K. Ounadjela, I.L. Prejbeanu, L.D. Buda, U. Ebels, M. Hehn, *Observation of micromagnetic configurations in mesoscopic magnetic elements*, in *Spin Electronics*, edited by M. Ziese, M.J. Thornton, Chap. 15 (Springer Verlag, Heidelberg, 2001), p. 332
25. M.J. Donahue, D.G. Porter, Oommf user's guide, Version 1.0, *Interagency Report NISTIR 6376*
26. R. Höhne, C.A. Kleint, A.V. Pan, M.K. Krause, M. Ziese, P. Esquinazi, J. Magn. Magn. Mater. **211**, 271 (2000)
27. M. Ziese, R. Höhne, P. Esquinazi, P. Busch, Phys. Rev. B **66**, 134408 (2002)
28. B.A. Calhoun, Phys. Rev. **94**, 1577 (1954)
29. T. Hughes, K. O'Grady, H. Laidler, R.W. Chantrell, J. Magn. Magn. Mater. **235**, 329 (2001)
30. L.E. Fernández-Outón, K. O'Grady, M.J. Carey, J. Appl. Phys. **95**, 6852 (2004)